

Flames

K. SAITO

Department of Mechanical Engineering, University of Kentucky, Lexington, Kentucky

- I. Introduction**
- II. Basic Aspects of Combustion in Forest Fires**
 - A. Governing Equations
 - B. Adiabatic Flame Temperature and Soot Formation
- III. Temperature, Velocity, Species Concentration, and Flame Height**
 - A. Temperature Measurement
 - B. Velocity Measurement
 - C. Species Concentration Measurement
 - D. Flame Height Measurement
- IV. Premixed and Diffusion Flames**
 - A. The Premixed Flame and Its Burning Velocity
 - B. Ignition
 - C. Ignition Temperature
 - D. Flammability Limits
 - E. Minimum Ignition Energy
- V. Extinction of Diffusion Flames**
- VI. Diffusion Flames and Scaling Analysis**
 - A. Re Number-Controlled Laminar Diffusion Flames with Low Pe Number
 - B. Re Number-Controlled Turbulent Jet Diffusion Flames with High Pe Number
 - C. Re and Fr Number-Controlled Laminar Diffusion Flames with Low Pe Number
 - D. Fr Number-Controlled Turbulent Diffusion Flames with High Pe Number
 - E. Scaling Laws
 - F. Wood Crib Fires
- VII. Spreading Flames**
 - A. Downward and Horizontal Flame Spread
 - B. Turbulent Upward Flame Spread
 - C. Flame Spread through Porous Fuel Beds
- VIII. Structure of Flame Base**
- IX. Conclusions**
- Notation**
- References**

I. INTRODUCTION

This chapter intends to help ecologists, forest fire researchers, and fire-fighting strategists understand some of the fundamental aspects of combustion and think scientifically about their forest fire problems. As with any discipline, the best approach to understanding forest fires is to grasp the fundamentals—in this case, the structure and behavior of flames. Explanation and discussion are based on the physical and chemical aspects of combustion, with little emphasis on strict mathematical treatment of equations. The chapter addresses basic knowledge on the structure of diffusion flames and scaling laws, premixed flames, ignition, diffusion flame extinguishment, spreading flames, and the mechanism of diffusion flame anchoring. Some general background in combustion research is introduced at the beginning.

Fire is the common name we give to high-temperature gaseous combustion. This combustion can occur in open land or an enclosed environment. In either case, regardless of the type of fire, two things are certain: heat is released, and the fire may spread. Flame is the fundamental element of fire that produces the heat and the combustion by-products (such as CO_2 , H_2O , CO , and smoke) by means of chemical reactions that occur between fuel and oxygen—called combustion.

Modern combustion research is composed of four theoretical supporting structures: thermodynamics, chemical kinetics, fluid mechanics, and transport processes (Williams, 1992). Additionally, three basic tools (experiment, theory, and computation) are available to help researchers approach combustion problems. Each tool has strengths and weaknesses.

Experiments have two roles: “insightful observation” and verification of assumptions that theory and computational methods employ (Hirano and Saito, 1994). The term “insightful observation” means to see things with unbiased minds using imagination and intuition. The second role of an experiment is well explained elsewhere in the scientific literature, while the first role is rarely emphasized, although it is important. In scientific research, the first and second roles often play together. For example, a simple experiment designed to verify assumptions also offers additional information to researchers. When a researcher conducts an experiment, two different points of view need to be kept in her or his mind: confirmation of assumptions and insightful observation. When the researcher’s mind is entirely occupied by the confirmation role only, she or he may miss the opportunity for discoveries and inventions through insightful observation. Our history proves that insightful observation is the source of discoveries and inventions (Ferguson, 1993).

Computation, also referred to as computer experiments, can provide detailed results and even a virtual reality by simulation. The combination of two

or more of these tools will increase not only the accuracy of the results but also the chance of getting correct answers, especially during the early stages of a research and development project (Wilson, 1954). Computational methods not only save time and energy of human calculation but also provide details of virtual reality under ideal initial and boundary conditions, which may be difficult to achieve by experiments.

II. BASIC ASPECTS OF COMBUSTION IN FOREST FIRES

“Combustion is exothermic (heat releasing) chemical reactions in flow with heat and mass transfer” (Williams, 1985; Linan and Williams, 1993). To be more specific, we can divide combustion into two types, based on the kind of chemical reaction and the flow regime (laminar and turbulent): high speed and low speed. Good examples of high-speed combustion are gas turbines, rocket motors, and internal combustion engines. Examples of low-speed combustion include forest fires and candle flames.

We can be more specific still by considering the type of flame in low-speed combustion. Forest fires, for example, burn with what are called diffusion flames. Diffusion flames can be maintained by a feedback loop; in the gas phase, heat is released by exothermic combustion of the secondary gaseous fuels, while in a condensed phase some of this heat is transferred back causing gasification of the primary fuel. Gasification is an endothermic (heat-absorbing) process that requires gaseous combustion in order to occur. This feedback of heat from the gas phase flames to the condensed phase fuels is an essential mechanism for sustaining the combustion process.

A. GOVERNING EQUATIONS

Governing equations or conservation equations can provide mathematically strict relationships among various quantities. In combustion science, conservation equations are partial differential equations expressing conservation of mass, momentum, energy, and chemical species. Derivation of conservation equations are detailed by Williams (1985) and Linan and Williams (1993) and are beyond the scope of this chapter; only the concept of these equations together with mathematical formulae for only mass and momentum conservation (because of their simple formulae) are explained.

By taking a volume element of flame fluid and assuming fluid velocity to be

much smaller than the speed of light, we can conceptualize the conservation equations for mass, momentum, energy, and chemical species as follows.

Mass Conservation:

$$\left[\begin{array}{c} \text{Rate of accumulation} \\ \text{of mass} \end{array} \right] + \left[\begin{array}{c} \text{Rate at which mass flows} \\ \text{into the volume element} \end{array} \right] = 0.$$

The mathematical expression is $\varpi \partial/\partial t + \nabla(\varrho \bar{u}) = 0$, where ϖ = ratio of flow time to evolution time, ϱ = density over characteristic density, and \hat{u} = velocity vector over characteristic velocity.

Momentum Conservation:

$$\left[\begin{array}{c} \text{Rate of increase} \\ \text{of momentum} \end{array} \right] = \left[\begin{array}{c} \text{Inertia} \\ \text{force} \end{array} \right] + \left[\begin{array}{c} \text{Pressure} \\ \text{force} \end{array} \right] + \left[\begin{array}{c} \text{Body} \\ \text{force} \end{array} \right] + \left[\begin{array}{c} \text{Viscous} \\ \text{force} \end{array} \right].$$

The mathematical expressions is $\varpi \partial(\varrho \bar{u})/\partial t = -\nabla(\varrho \bar{u} \bar{u}) - \nabla p/M^2 + F/Fr + \nabla Ts/Re$, where p = pressure over characteristic pressure, M = Mach number, F = body force, Fr = Froude number, Re = Reynolds number, and Ts = shear stress tensor.

Energy Conservation:

$$\left[\begin{array}{c} \text{Thermal} \\ \text{energy} \end{array} \right] + \left[\begin{array}{c} \text{Chemical} \\ \text{energy} \end{array} \right] + \left[\begin{array}{c} \text{Kinetic} \\ \text{energy} \end{array} \right] \\ + \left[\begin{array}{c} \text{Energy lost by conduction} \\ \text{and radiation} \end{array} \right] + \left[\begin{array}{c} \text{Work done on} \\ \text{surroundings} \end{array} \right] = \text{Constant}$$

Chemical Species Conservation:

$$\left[\begin{array}{c} \text{Accumulation} \\ \text{rate of given} \\ \text{chemical species} \end{array} \right] = - \left[\begin{array}{c} \text{Convection of the} \\ \text{chemical species out} \\ \text{of the volume element} \\ \text{by fluid motion} \end{array} \right] + \left[\begin{array}{c} \text{Diffusion of} \\ \text{the species into} \\ \text{the volume} \\ \text{element} \end{array} \right] \\ + \left[\begin{array}{c} \text{Production of the} \\ \text{chemical species} \\ \text{by chemical} \\ \text{reactions} \end{array} \right]$$

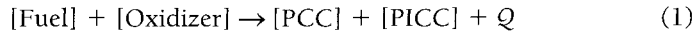
The conservation (mass and energy) equations are often applied to the condensed phase.

When these conservation equations are solved under specified boundary and initial conditions, they can provide predictions on changes of pressure, velocity, temperature, and chemical species as a function of time and space. Linan and Williams (1993) point out that no combustion problems require the full

description of all the terms in the conservation equations and recommend the simplification of combustion phenomena. For combustion of solids, which includes most forest fires, for example, the phenomenological derivation is more satisfying than the first principle approach of using these complete conservation equations. Here, phenomenological derivation means to come up with empirical equations using experimental data and physical principles, but not starting from the basic governing equations.

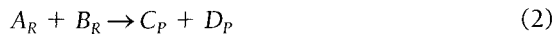
B. ADIABATIC FLAME TEMPERATURE AND SOOT FORMATION

The most desirable condition for combustion would be to reach the adiabatic flame temperature, the ideal maximum temperature that a combustion system can attain. In such a case, we would have no heat loss from the system. However, real systems don't reach this point because the actual combustion process consists of finite-rate chemical reactions with heat loss that occurs in the forms of convection, radiation, and conduction. All these losses contribute to leading the combustion system to incomplete combustion. Incomplete combustion produces products of incomplete combustion (PICCs). Common examples of PICCs include CO, NO_x, SO_x, dioxin, all kinds of intermediate hydrocarbons (C_nH_m, where *n* and *m* = 1, 2, 3, . . .) and soot (solid particulates). The following diagram describes the generic process of combustion:



where PCC are the products of complete combustion. When complete combustion occurs in an adiabatic system, no PICCs are formed, the heat of combustion *Q* reaches a maximum, and the system achieves adiabatic flame temperature. For example, adiabatic flame temperature for a methane + air reaction is 1875°C and that for most hydrocarbon + air systems falls between 1800°C and 2200°C. The detailed procedure to calculate adiabatic flame temperature is straightforward (e.g., Glassman, 1996) using the JANAF Thermochemical Tables (1985).

Flame temperature for an incomplete combustion system can also be calculated by assuming incomplete combustion products. Computer programs (e.g., NASA's Gordon and McBride and STANJAN, see Glassman, 1996) are available to calculate the flame temperature and equilibrium compositions. Equilibrium compositions, defined as species concentrations at a specified temperature, can be calculated using the equilibrium constant that is available in the JANAF Table. For example, an arbitrary second-order reaction can be written as



where A_R and B_R are reactants and C_P and D_P are products. A simple example is



The reaction rate describing how quickly a given reactant, A_R , for example, disappears and converts to the product can be written using the Arrhenius approximation:

$$-d[A_R]/dt = -k[A_R][B_R] = d[C_P]/dt = -A \exp(-E/R_0T)[A_R][B_R] \quad (4)$$

where [] means concentration, t is time, k is specific reaction rate constant, A is preexponential factor, E is activation energy, R_0 is universal gas constant, and T is temperature. The values of k , E , and A have been studied for many different types of hydrocarbon-air combustion systems and are available in the literature (e.g., Glassman, 1996). For further information regarding chemical kinetics, see Benson (1960) and Glassman (1996).

For combustion efficiency, the ratio of the actual heat release to the maximum ideal heat of combustion ranges from 50 to 95% (Pyne *et al.*, 1996). The combustion efficiency can be defined more specifically as the ratio of the actual carbon contained in the emissions of carbon dioxide compared to that theoretically possible, assuming that all the carbon was released as carbon dioxide. Under such combustion efficiency, many PICCs will be formed. As a result, for such a system, the temperature drops a few hundred degrees below the adiabatic flame temperature. However, there is a critical extinction temperature beyond which flame won't exist. A universal value of extinction, approximately 1300°C (Rashbash, 1962), was found for cellulosic fuels.

Soot is a typical PICC and has a large impact on the environment when it is formed in the case of forest fires by degrading ambient air quality, impairing visibility, worsening regional haze, and causing significant health problems (Pyne *et al.*, 1996, and Chapter 3 in this book). Therefore, a brief explanation of soot formation and properties will be given here. When soot is formed in a high-temperature flame zone, it emits a luminous yellow (black body) radiation; when it escapes from the flame, it can be seen as a cluster of small black particles. Smoke is a rather large cluster of soot particles (100 μm or larger) and is usually large enough for human eyes to recognize, while no clear-cut distinction is made between smoke and soot.

Scanning electron microscopy (SEM), transmission electron microscopy (TEM), electron spectroscopy for chemical analysis (ESCA), and laser desorption mass spectrometry (LDMS) have been used to investigate the physical and chemical structures of soot.

Soot can be collected directly from the hot flame zone by different direct sampling techniques (Fristrom and Westenberg, 1985): (1) a filter paper to collect soot through a vacuum line, (2) a small quartz needle and a stainless-steel

mesh-screen to be inserted into a flame to deposit soot on them (Saito *et al.*, 1991), and (3) a thermophoretic sampling probe to collect soot (Dobbins and Megaridis, 1987). Technique (1) is suitable for measuring an average amount of soot produced in a relatively long time period (roughly an order of 10s or greater). The two other techniques are suitable for detailed chemical analysis. The residence time of technique (2) is roughly an order of a few seconds or greater, and that of technique (3) is roughly 50 milliseconds. Technique (2) provides a layer of soot deposit to be analyzed with little effect of heterogeneous catalysis on the soot and probe material. Technique (3) can provide individual soot particles that are collected by inserting a thermophoretic probe directly into a flame. Soot in the flame is attracted by copper and other metal grids by thermophoresis.

Most of the soot studies were conducted for laboratory scale candlelike laminar diffusion flames because they allow researchers easy access to laser optics and other measurement systems that require well-controlled laboratory conditions. These studies found that soot is actually a cluster consisting of small primary soot particles. The average diameter of the mature primary soot particle produced by small laminar diffusion flames was identified by a scanning electron microscope and a transmission electron microscope to be approximately 20 to 50 nm ($1 \text{ nm} = 10^{-9} \text{ m}$). The average molecular weight of soot is 10^6 g/mole , and the C/H ratio is 8 to 10 (Glassman, 1996). The mechanism of primary soot-particle formation, however, is not well understood. Two competing mechanisms that have been proposed recently include: (1) a gradual buildup of a carbonaceous product via formation and interaction of polycyclic aromatic hydrocarbons (PAHs) or acetylene (C_2H_2) molecules through dehydrogenation and polymerization processes, and (2) a direct condensation of liquidlike carbonaceous precursor materials to form a solidlike precursor soot particle as a result of fuel pyrolysis reaction, polymerization, and dehydrogenation.

Regarding the soot and smoke formation mechanisms, there is a belief that, because soot is formed in the gas phase during the process of fuel pyrolysis, difference in fuel type (either gas or liquid or solid) has little influence on soot formation processes. This may be true for the physical shape of primary soot particles which are spherical. However, a recent laser-desorption mass-spectroscopy study (Majidi *et al.*, 1999) showed that mature soot collected from several different laminar hydrocarbon-air diffusion flames have different in-depth chemical structures. This is interesting because, if it is proved true for a wide range of fuels, soot could be used to identify its parent fuel, helping in fire investigations. No LDMS data are available for soot collected from forest fires.

A few studies focused on smoke generated from liquid pool fires. Fallen smoke particles were collected on the ground (Koseki *et al.*, 1999; Williams and Gritzo, 1998) or sampled at a post flame region by an airborne-smoke-sampling package (Mulholland *et al.*, 1996). They used crude oil fires whose diameters

ranged from 0.1 to 20 m and sampled smoke particles generated by these fires; primary smoke particles from these crude oil fires looked spherical, and the primary particle diameters varied between 20 and 200 nm depending on the sampling location and diameter of the pool. These studies found a general trend: the larger the fire, the larger the primary smoke particle, suggesting the observed result may be attributable to the longer resident time.

The smoke generation rate from many different types of solid fuels was tested using a laboratory scale apparatus. When small solid samples were exposed under constant heat flux, they increased their temperature, released pyrolysis products and eventually emitted smoke. The amount of smoke can be measured by a light-scattering device or can be collected on a filter paper for weight measurement. When a pilot ignitor is placed over the sample, the sample can be ignited to study material flammability and flame spread characteristics (Fernandez-Pello, 1995; Kashiwagi, 1994; Tewarson and Ogden, 1992; Babrauskas, 1988). The flame spread occurs in horizontal, upward, and downward directions with and without an external (radiation) heat source. These kinds of experimental apparatus require relatively small samples (e.g., 10 cm wide \times 30 cm long for flame spread tests, Saito *et al.*, 1989), but some of them are designed for large scale upward spread tests (Orloff *et al.*, 1975; Delichatsios *et al.*, 1995). Effects of sample size and geometrical shape on ignition, flammability and flame spread rate are not well understood (Long *et al.*, 1999). Caution should be taken when the laboratory test results are applied to evaluate behavior of forest fires that involves many different types, kinds and sizes of trees, and bushes and duff in the forest.

III. TEMPERATURE, VELOCITY, SPECIES CONCENTRATION, AND FLAME HEIGHT

Measurements of flame temperature, velocity, height, and chemical species concentrations are important for understanding the structure and characteristics of forest fires. The first three quantities can be measured at a point and thus allows determination of profiles. Height can be measured as the time-averaged maximum height of the yellow flames since it is most relevant to radiant heat released from the flame.

For the first three quantities, profile data can provide more information than point data, but any (one-, two-, and three-dimensional) profile data require more human effort and better (often more sophisticated) equipment than point measurement. The profile data provide us with the relative change of the measured quantity (such as temperature), thus helping us better understand fire phenomena.

A. TEMPERATURE MEASUREMENT

Temperature measurement with thermocouples is the most commonly used flame temperature measurement technique. It is an intrusive point-by-point measurement and is affected by radiation (q_{rad}), convection (q_{cov}), and conduction (q_{cod}) heat losses. These heat losses can be described in terms of heat flux: $q_{\text{rad}} \sim \varepsilon_b \sigma T_b^4 (1 - a)$; $q_{\text{cov}} \sim \dot{\eta} (T_b - T_a)$; $q_{\text{cod}} \sim \lambda (T_b - T_a) / l_T$. Here, ε_b = emissivity of the thermocouple bead, a = absorption coefficient of the gas surrounding the thermocouple, σ = Stefan-Boltzmann constant, T_b = thermocouple bead temperature, T_a = gas temperature surrounding the thermocouple bead, l_T = a characteristic length related to the high-temperature gradient in the gas, $\dot{\eta}$ = heat transfer coefficient, and λ = thermal conductivity of gas. To minimize these heat losses, a thermocouple with a small bead and a small wire diameter is advantageous. To minimize the conduction heat loss, the wire can be placed along an isotherm in the flame. Radiation heat loss proportional to the fourth power of temperature may become dominant above 1000°C. Soot deposit on the thermocouple junction changes the thermocouple output reading due to the change in emissivity of the junction. A sheathed thermocouple is available to minimize the radiation effect. When a bare thermocouple is used, caution should be taken for the measurement on sooty flames because the fire-generated smoke and soot can coat the thermocouple bead quickly and change its emissivity, increasing the radiation heat loss. An extrapolation to zero insertion time can be used to eliminate the soot-coating effect on the thermocouple (Saito *et al.*, 1986). When thermocouples are used for field tests, a lead wire that connects the thermocouple and its detector should be as short as possible and lifted above ground to avoid a short circuit due to an accidental step or contact with water. The lead wire should be covered by a heat-insulating material to prevent convective heat loss when significant convective heat loss is expected.

The infrared thermograph technique involves use of an infrared camera and an image recording and analysis system capable of obtaining a two-dimensional thermal image from a remote location. This technique was applied to measure upward flame spread rate on wood slabs (Arakawa *et al.*, 1993) and temperature profiles in forest fires (Clark *et al.*, 1998; 1999). Radke *et al.* (1999) applied an airborne imaging microwave radiometer to obtain a real-time airborne remote sensing. These techniques can be very useful in identifying the hot spot or pyrolyzing condensed-phase front which can be related to the active flame spread front. Note that the infrared technique may not represent exactly the actual temperature of the flame or condensed phase because the phase emissivities vary from location to location and because absorption by smoke, H₂O, and CO₂ will influence the infrared signal. Arakawa *et al.* (1993) suggest the use of a band-pass filter ($10.6 \pm 0.5 \mu\text{m}$) to eliminate the absorption effects of these gases.

A color video camera may be used to obtain relative flame temperature change in forest fires because the flame color can be roughly related to the flame temperature. The color video camera technique is simple and useful for seeing relative change throughout the flame, but it is more qualitative than the infrared thermograph. Combination of the thermocouple, infrared thermograph, and color video camera techniques may be most ideal for researchers to assess flame temperature correctly.

Other temperature measurement procedures that are mainly suitable for laboratory-scale flames include the holographic interferometer (Ito and Kashiwagi, 1988), two-color pyrometer (Gaydon and Wolfhard, 1979), spectrum-line reversal method (Gaydon and Wolfhard, 1979), and coherent anti-Stokes Raman spectroscopy (Demtroder, 1982). The two-color pyrometer employs two different wavelength band-pass filters to eliminate emissivity of the object. It is suitable to measure from a remote location a local temperature of sooty-yellow flames whose profiles are fairly uniform along the direction of measurement. Typical examples are combustion spaces of internal combustion engines and boilers. All other techniques are based on a laser optic system which requires a dark room and accurate alignment. These systems are sensitive to environmental change and not suited to field measurements.

B. VELOCITY MEASUREMENT

A pitot tube velocity measurement is a commonly used velocity measurement technique. It is an intrusive and point-by-point measurement (Sabersky *et al.*, 1989). Pitot tubes can accurately measure velocity in the range of a few meters per second to above 100 m/s, covering most of the wind velocity range in forest fires. The pitot tube is relatively simple and can measure a one-dimensional velocity component, but it also can be applied to a three-dimensional measurement by changing the direction of the pitot tube head when the flow is at steady state.

A simple velocity measurement technique with practical use is a video camera. Recording the fire behavior in a video camera and reviewing it on a monitor screen, researchers may be able to trace the trajectory of smoke and fire brand particles moving in and over the fire area and calculate approximately the local velocity as well as two dimensional velocity profiles. This technique is qualitative at best because the smoke and particles may not exactly follow the flow stream and also the flow may be complex and three-dimensional. Wisely using the video image, however, researchers can gain valuable information on the approximate flow velocity in relation to the overall fire behavior.

Other available velocity measurement techniques, all of which are laser-based

methods and only suitable to laboratory experiments, include laser doppler velocimetry (LDV) and particle image velocimetry (PIV) or laser sheet particle tracking (LSPT). LDV is a point-by-point measurement, and PIV and LSPT are capable of measuring two-dimensional, and possibly three-dimensional velocity profiles. All three of these techniques require seeding of small trace particles, laser optics, and a data acquisition system. An example of these techniques applied to flame base structure is shown later.

C. SPECIES CONCENTRATION MEASUREMENT

Gas chromatography is the most commonly used method of analyzing the concentration of species, such as CO_2 , CO , H_2O , N_2 , O_2 , and many different hydrocarbons. A sampling probe collects sample gases by means of either a batch or continuous flow system. The batch sampling requires transport of the sample to a laboratory where the samples will be analyzed. The continuous flow system offers an on-line analysis at the site. The continuous flow system is better than the batch sampling system because the on-line method eliminates the possibility of sample contamination during transportation and storage. For field experiments, portable gas analyzers can be used for the on-line measurement of concentrations of some or all the following species: O_2 , N_2 , CO_2 , H_2O , CO , NO_x , and other hydrocarbons. These instruments require frequent calibration. Their sensitivity and response time should satisfy the required accuracy of each experiment.

A quartz microsampling probe is commonly used for sampling of laboratory-scale flames. It consists of a tapered quartz microprobe with a small sonic orifice inlet which accomplishes rapid cooling and withdrawal of the sampling gas by adiabatic expansion (Fristrom and Westenberg, 1985). During the measurement of water concentration, the sampling line should be heated above the dew point to prevent water condensation; this is called wet-base sampling. Another method is dry-base sampling in which all water is removed before analysis. The dry-base technique requires a water condensation unit in the sampling line. A water-cooled stainless-steel sampling probe is often used to provide dry-base sampling of large scale fires. When an uncooled probe is used for dry-base measurement, a water condensation unit is needed to be sure all water is removed before analysis. The sampling line that connects the probe and the batch (or the probe and the analytical instrument) should be free from contamination by left-over gas or air leaks. The commonly used sampling line materials are Teflon, quartz, and stainless steel.

The previously mentioned sampling techniques are intrusive and provide time-average species concentrations within a specific sampling volume. Physical

disturbances due to the probe may be negligible for forest fires, but they may become important for small-scale laboratory flames. For further information, see Fristrom and Westenberg (1985).

D. FLAME HEIGHT MEASUREMENT

The purpose of flame height measurement is to estimate radiation intensities from the flame, an important parameter for assessing hazards to personnel and the rate of flame spread. The most widely accepted interpretation of flame height is the height where the flame achieves the maximum temperature. Another definition that has more practical application to forest fires is the vertical distance from the flame base to the yellow visible flame tip. These two definitions may not always give the same flame height. For a small candle flame the maximum temperature is near the visible yellow flame tip, while for a 1-m diameter crude oil fire the maximum temperature is achieved at about two thirds of the time-averaged visible flame height, probably because a fire-induced strong turbulent air flow cools the upper portion of the 1-m diameter fire.

Here, two different methods of determining flame height will be introduced. The first is to measure the visible flame tip, and the second is to identify the location of the maximum flame temperature. The values obtained by these techniques are valid to within $\pm 10\%$ uncertainty.

To measure the time-average visible yellow flame height, a motor-driven 35mm still camera or a motion color video camera can be used. Both are capable of measuring temporal flame behavior from which time-averaged flame height can be measured. The latter equipment has an advantage in accuracy because it offers the measurement of flame height over the slow motion video screen. For a smoke-covered flame, however, neither technique is applicable because the flame tip is invisible. For these types of fires, an infrared camera can be used to penetrate the smoke layer and measure the maximum flame temperature location. Caution is required when the infrared camera is used to identify the maximum flame temperature and/or visible flame tip because emissivity of the flame is unknown, and it varies with fuel and location in the flame.

Figure 1 is a simplified plot of dimensionless flame height (visible flame height divided by a horizontal scale of fire) as a function of dimensional parameter measuring Froude number (the ratio of inertia force to buoyancy force) (Williams, 1982). The error bars in the correlation are due to different measurement techniques, different fuels, and different flame height definitions. However, the correlation itself is reasonably high over the 15 orders of magnitude in Froude number and the 6 orders of magnitude in the ratio of flame height to the fuel-bed dimension.

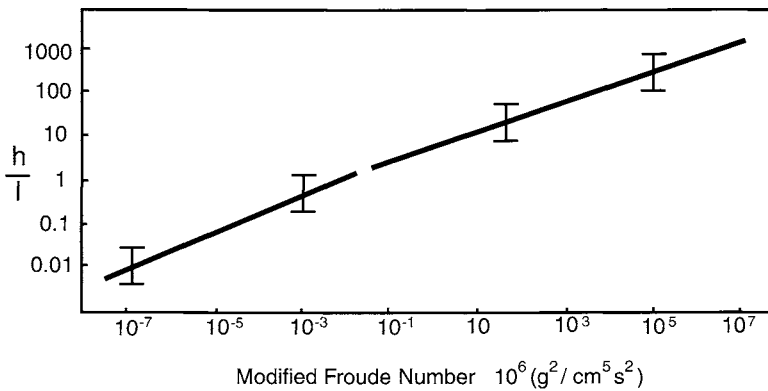


FIGURE 1 Dimensionless flame height as a function of modified Froude number (Williams, 1982). Quantity l is a horizontal scale of the fire.

IV. PREMIXED AND DIFFUSION FLAMES

The idea of categorizing flames into two different types, premixed and diffusion flames, and then studying each type thoroughly has proven to be successful. Many studies have contributed to a thorough understanding of these two types of flames. Based on these studies, much progress has been made in the field of combustion (Williams, 1985; Linan and Williams, 1993; Glassman, 1996; Hirano, 1986). Although diffusion flames can represent forest fires, the premixed flame allows us to better understand the diffusion flame by comparing its structure with that of premixed flames. Thus, in this chapter, characteristics of both diffusion and premixed flames are explained. However, note that these concepts are by no means perfect and may not be applicable to all forest fire phenomena. For example, the microstructure of a flame's leading edge can be interpreted by using a different concept (Venkatesh *et al.*, 1996).

A diffusion flame is defined as any flame in which the fuel and the oxidizer are initially separated. Diffusion flames are represented by candle flames, match flames, wood fires, and forest fires. A premixed flame is defined as any flame in which the fuel and the oxidizer are initially mixed. A good example of a premixed flame is a uniform combustible mixture contained inside a tube that is ignited by a spark creating a flame spreading along the tube (Williams, 1985). The most significant difference between diffusion and premixed flames is that in the former the fuel-oxidizer ratio varies throughout the flame, whereas in the latter it is constant everywhere in the flame. Some flames possess both characteristics, and they will be called partially premixed flames.

According to the flow regime, both diffusion and premixed flames can be classified as laminar, turbulent, or transitional. Laminar flames have smooth, steady flow characteristics in and around the flame, whereas turbulent flames have irregular, disorganized flow characteristics in and around the flame. The use of Reynolds number (the ratio of viscous force to the inertia force) for judging flames to be either turbulent or laminar is not always straightforward because of uncertainty involved in determining characteristic parameters; a visual observation is often good enough to make this judgment. Some flames may be laminar in one section and turbulent in the other section (e.g., the flame shape in a 1-m diameter crude oil fire is turbulent except at the flame base where the flame anchors and flame shape is laminar). In the following discussion, premixed flames and four different types of diffusion flames will be explained.

A. THE PREMIXED FLAME AND ITS BURNING VELOCITY

One important characteristic of the premixed flame is the burning velocity. Assuming the pressure p constant, and with the specific heat c_p of the mixture taken as constant, the overall energy conservation shows that the energy per unit mass added to the mixture by the combustion, H_0 , is

$$H_0 = c_p(T_\infty - T_0) \quad (5)$$

where T_0 and T_∞ are the initial and final temperature, respectively. This energy can be determined by the rate of conversion of reactant mass to product mass. Using Eq. (4), this conversion rate (mass per unit volume per unit time) can be written as

$$w = AY_F^m Y_O^n \exp(-E/R_0T) \quad (6)$$

where the subscripts F and O identify fuel and oxidizer, the mass fractions Y_F and Y_O are proportional to the concentrations (the number of molecules per unit volume) of the reactants, and m and n are the overall reaction orders with respect to fuel and oxidizer, respectively. In terms of the thickness δ of the flame, the chemical energy released per unit area per unit time may be approximated as

$$H_0 w \delta = \lambda(T_\infty - T_0)/\delta \quad (7)$$

where λ is the thermal conductivity.

Using Eqs. (5) and (7) and solving for δ , we obtain

$$\delta = [\lambda/(c_p w)]^{1/2} \quad (8)$$

which shows that the flame thickness varies inversely with the square root of the reaction rate. The mass of reactant converted per unit area per unit time is $\rho_0 v_0$, where ρ_0 is the initial density of the mixture and v_0 is the laminar burning velocity. By conservation of fuel mass in the steady flow, we have

$$\rho_0 v_0 = w\delta \quad (9)$$

Using Eqs. (8) and (9), the laminar burning velocity takes the form

$$v_0 = (1/\rho_0)[(w\lambda)/c_p]^{1/2} \quad (10)$$

Equation (10) shows that the laminar burning velocity is proportional to the square root of the ratio between the diffusivity, $\lambda/(c_p\rho_0)$, and the reaction time, ρ_0/w . Equation (10) agrees with laminar flame spread experiments using a vertical tube filled with a fuel and oxidizer mixture. When the mixture is ignited, a steady laminar flame spread occurs from the top to the bottom. The flame spread rate can be measured fairly accurately using a motor-driven camera or a high-speed video camera or an array of thermocouples placed along the inner surface of the tube.

B. IGNITION

Ignition can be achieved either by heating the system containing a combustible mixture with thermal energy or by creating chain reactions with autocatalytic reactions. Chemical reactions whose reaction rate is controlled by the concentration of initially present reactants are called thermal, whereas reactions whose rate is affected by the concentrations of the intermediate and final products are called autocatalytic.

Thermal ignition can be achieved by supplying an external source of heat to the system. An electric arc, a spark plug, or a pilot flame can be the external heat source. The external heat source provides excess heat to the system and raises its temperature continuously if the heat input exceeds the heat loss. At some point, the temperature rise will become highly accelerative and a high heat evolution will occur. This is called ignition.

Autocatalytic ignition can be achieved by increasing the rate of chain carrier generation over the termination reaction of chain carriers. The initiation of chain carrier generation may be achieved by thermal energy. After the initiation reaction has started, the reaction may become self-accelerative even after the external heat is removed. Then the system will ignite by satisfying the self-sustaining condition. Lightning may be a good example of autocatalytic ignition.

An important topic in forest fires is determining the condition under which given combustible forest materials can ignite. There are two types of ignition—

spontaneous (unpiloted) ignition and piloted ignition. Unpiloted ignition can be achieved by raising the temperature of the system with hot boundaries and adiabatic compression. Piloted ignition can be achieved by adding heat to the system with an external heat source. Ignition temperature (explained later) for unpiloted ignition is higher than for piloted ignition. For example, ignition temperature for piloted ignition of cellulose is approximately 350°C, whereas that for unpiloted ignition is approximately 500°C (Williams, 1982).

Other important aspects of ignition related to forest fires include ignition temperature, flammability limits, and minimum ignition energy.

C. IGNITION TEMPERATURE

Ignition temperature can be defined as the critical temperature that the condensed phase needs to achieve for burning to begin (Williams, 1985). The ignition temperature is a useful criterion to assess the flammability of materials and estimate flame spread rate. However, there are some variations among different ignition conditions. For example, some researchers use a black body as the heating source, and others use a halogen or infrared lamp (Babrauskas, 1988).

Ignition tests conducted in an inert atmosphere under various external heat flux conditions showed that the ignition temperature indeed varies as a function of external radiant heat flux. The higher the external heat flux, the higher is the ignition temperature (Delichatsios and Saito, 1991). Thus, some caution should be taken when laboratory ignition temperature data are applied to forest fire problems.

D. FLAMMABILITY LIMITS

If there is too little or too much fuel in a fuel-air mixture, ignition may not occur even if a pilot flame provides sufficient heat to the mixture. For example, a propane + air mixture with fewer than 2.2 mole of propane or more than 9.5% of propane can't ignite. The maximum and the minimum concentrations of fuel within which flame can spread are called, respectively, rich and lean limits of flammability. Flammability limits depend on pressure and temperature; such data for gases are well established (Zabetakis, 1965). Flammability of solid fuels can be linked to ignition of solids that release pyrolysis products under external heating. These pyrolysis products will mix with air forming a flammable mixture whose flammability can be tested. Thus, knowledge gained through studies on flammability limits for gases can be applied to understand the flammability of solids.

E. MINIMUM IGNITION ENERGY

Williams (1985) offers a simple and practically useful definition of minimum ignition energy. "Ignition will occur only if enough energy is added to the gas to heat a slab about as thick as a steadily propagating adiabatic laminar flame to the adiabatic flame temperature." Thus, the minimum ignition energy, H , can be described by

$$H = (\tilde{A}\delta)\rho_0[c_p(T_\infty - T_0)] \quad (11)$$

where \tilde{A} is the cross-sectional area of the slab, δ is the adiabatic laminar flame thickness, ρ_0 is the initial density of the mixture, c_p is the average specific heat at constant pressure, T_∞ is the adiabatic flame temperature, and T_0 is the initial temperature of the mixture. Using $\delta \approx \lambda/c_p\rho_0v_0$ (Williams, 1985), Eq. (11) can be written as

$$H/\tilde{A} = \lambda(T_\infty - T_0)/v_0 \quad (12)$$

where λ is the average thermal conductivity of the gas and v_0 is the laminar burning velocity discussed earlier.

V. EXTINCTION OF DIFFUSION FLAMES

There are two main flame extinction criteria: the Damköhler extinction criterion and the Zel'dovich extinction criterion, both of which were detailed by Williams (1985) and Linan and Williams (1993). Here a summary of the Damköhler extinction criterion is presented.

Extinction can be defined as a balance between a chemical time, t_c , and a residence time, t_r , in the gas-phase flames. A nondimensional parameter known as Damköhler number, Da , is defined as the ratio of a flow (or diffusion) to chemical reaction times in the gas:

$$Da \text{ number} = (\text{A flow or air diffusion time})/(\text{Chemical reaction time}) = t_r/t_c \quad (13)$$

Using the chemical time, $t_c = AY_F Y_O \exp(E/R_0T)$, and the residence time, $t_r = l/u$ or l^2/α , Eq. (13) can be written as

$$\begin{aligned} Da \text{ number} &= (l/u)(AY_F Y_O)^{-1} \exp(-E/R_0T) \\ \text{or} & \quad (l^2/\alpha)(AY_F T_0)^{-1} \exp(-E/R_0T) \end{aligned} \quad (14)$$

where u is the characteristic flame velocity, l is the characteristic length, α is the thermal diffusivity of the gas, and $m = n = 1$ denoting the first-order chemical reaction.

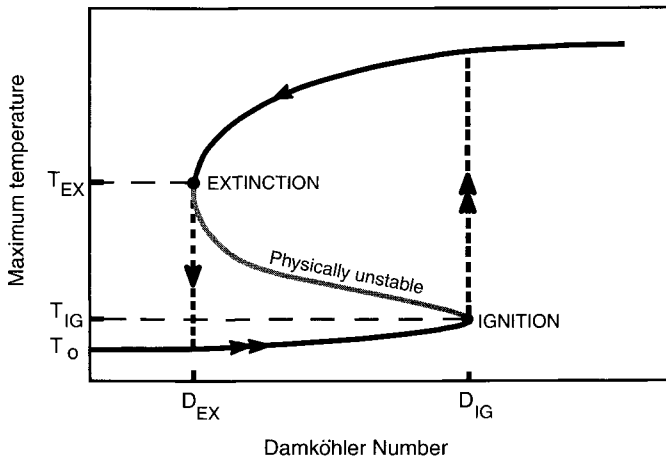


FIGURE 2 Schematic illustration of the dependency of the maximum temperature on the reduced Damköhler number for diffusion flames. Here, for cellulose-based fuels, T_{EX} (extinction temperature) = $1300 \pm 100^\circ\text{C}$, T_{IG} (ignition temperature) = $350 \pm 50^\circ\text{C}$, and T_0 (initial fuel temperature) = 20°C .

The maximum temperature can be taken as an important parameter to control extinction. Figure 2 shows temperature as a function of the Da number, a well-known S-shaped curve. Variation of parameters that control fires causes the Da number to change continuously. For example, if the Da number based on T_0 is increased beyond the critical Da number marked as ignition (D_{IG}), then a discontinuous change to a much higher temperature will occur (this passage is shown in a double arrow). If the upper branch of the Da number is decreased continuously to the critical Da number marked as extinction (D_{EX}), then a discontinuous change to a lower temperature will occur (this passage is shown in a single arrow). At the lower branch temperature, there is no combustion, whereas at the upper branch temperature, active combustion is taking place. The middle branch is unstable and not physically relevant. The Damköhler extinction criterion is useful in obtaining overall chemical kinetic parameters for gas-phase combustion from experimental data.

There are eight different strategies to achieve extinction: isolate the fuel, isolate the oxidizer, cool condensed phase, cool the fuel, cool the gas, inhibit the chemical reaction homogeneously, inhibit chemical reaction heterogeneously, and blow the flame away (Williams, 1982).

The Zel'dovich extinction criterion, derived by assuming a large activation energy asymptote (Linan and Williams, 1993), is beyond the scope of this book. Readers who are interested in the Zel'dovich extinction criterion may consult Linan and Williams (1993).

VI. DIFFUSION FLAMES AND SCALING ANALYSIS

Diffusion flames can be classified based on the forces that control the flow and mixing processes. The major forces acting on the diffusion flames may be assumed to include momentum, viscous, and buoyancy forces. Molecular diffusion driven by concentration differences is also assumed to play an important role in the mixing process. Based on these assumptions, scaling analysis (Williams, 1969; Emori and Schuring, 1977) can be conducted to categorize the diffusion flames into four different types. Scaling laws are important in fire research as described in the scaling law section later in this chapter. By defining u_0 = the fuel exit velocity, d = the burner port diameter, D = the binary diffusion coefficient of a fuel into air, g = the acceleration due to gravity, and ν = the kinematic viscosity, the following three pi-numbers (dimensionless numbers) can be formed when a fire burns in calm air:

- Peclet (Pe) number = [Fuel mass transferred by momentum of incoming fuel flow]/[Fuel mass transferred by concentration difference] = $u_0 d/D$
- Reynolds (Re) number = [Momentum force of incoming fuel flow]/[Viscous force of air and fuel] = $u_0 d/\nu$
- Froude (Fr) number = [Momentum force of air induced by the flame]/[Buoyancy force in the flame] = u_0^2/dg

Here four different types of flames, each identified by different combinations of the preceding three pi-numbers, will be discussed.

A. Re NUMBER-CONTROLLED LAMINAR DIFFUSION FLAMES WITH LOW Pe NUMBER

Consider the case of a hypodermic needle held vertically and in which a hydrocarbon fuel constantly flows through the bottom end to the top. When the fuel is ignited, a small laminar diffusion flame with flame height of a few millimeters is established on the port of the hypodermic needle. This flame is called a microdiffusion flame. The existence of this type of flame was predicted by Williams (1985) and proven experimentally by Ban *et al.* (1994). It is governed by the balance between the momentum of the incoming fuel flow and the molecular diffusion (both in axial and radial directions) of the gaseous fuel and air. The shape of a microdiffusion flame is spherical and different from the more commonly observed candlelike diffusion flame.

The momentum and species equations are coupled, and a similarity solution has been obtained for the coupled system. Microdiffusion flame experiments on CH_4 , C_2H_2 , and C_2H_4 were conducted under ambient atmospheric

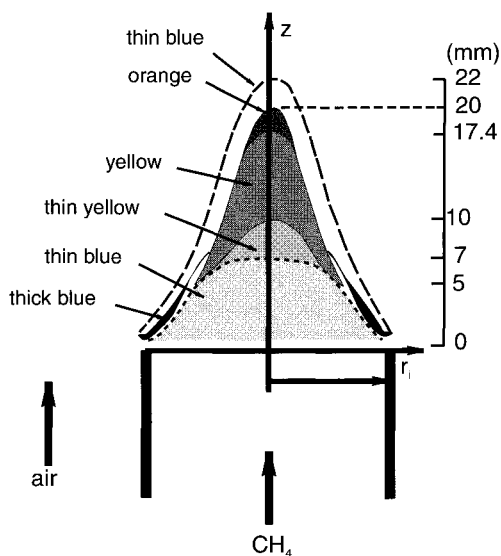
pressure conditions. Flame shape was photographically recorded and compared well with the theoretical predictions. Figure 3 (see color insert) shows a photograph and a schematic of an ethylene-air microdiffusion flame established on a 0.25-mm-diameter hypodermic needle (Ban *et al.*, 1993).

B. Re NUMBER-CONTROLLED TURBULENT JET DIFFUSION FLAMES WITH HIGH Pe NUMBER

By increasing the incoming fuel velocity in the previously mentioned hypodermic needle, the flame will become unstable, and at some point the flame can no longer be sustained at the burner port. This is because the characteristic time of the incoming fuel velocity is smaller than the time required for the flame to complete the chemical reaction. By increasing the diameter of the burner, a stable flame with a higher Re number can be achieved. For example, a hydrogen jet diffusion flame can be stabilized on a 1.43-mm-diameter nozzle burner up to $Re = 4800$, and a methane jet diffusion flame can be stabilized on a 9.45-mm-diameter nozzle burner up to $Re = 8440$ (Takahashi *et al.*, 1996). Figure 4 (see color insert) shows a hydrogen-air turbulent jet diffusion flame stabilized on the 1.43-mm-diameter burner (Takahashi *et al.*, 1996). For turbulent jet diffusion flames, the flame will be established as the result of the mixing of the incoming fuel jet with quiescent air. The momentum force controls the fuel jet, and the inertia and viscous forces of both the air and the fuel control the mixing process. This type of flame (high Pe and Re numbers) is stabilized by a turbulent shear mixing, but not by molecular diffusion (Takahashi *et al.*, 1996; Venkatesh *et al.*, 1996).

C. Re AND Fr NUMBER-CONTROLLED LAMINAR DIFFUSION FLAMES WITH LOW Pe NUMBER

Applying a relatively slow fuel flow rate (approximately a few centimeters per second) to the burner with a diameter of a few millimeters to a few centimeters, a candlelike flame can be established over the burner port. This is the regime of buoyancy-controlled laminar diffusion flames. Buoyancy forces acting on the hotter, less-dense gas in the region of the flame often distort the shape of the flame sheet. Figure 5 shows a candlelike laminar methane-air diffusion flame established on a 1.6-cm-diameter Pyrex burner. Faraday (1993, originally published in 1861) was the pioneer to identify this type of diffusion flame as the most basic type and conducted a series of noble experiments. After Faraday,



A small laminar methane - air diffusion flame

FIGURE 5 A schematic of a small methane-air diffusion flame established on a 1.6-cm diameter Pyrex tube (the average fuel flow rate at the burner port is 2.2 cm/s and the air flow rate is 9.3 cm/s).

many researchers have used this type of diffusion flame to further understand their chemical, thermal, and fluid mechanical structures. These flames are also ideal for optical and chemical species sampling measurements because they are stable, steady, and large enough to obtain accurate measurements.

The structure of laminar diffusion flames in this category is also of current interest for a number of reasons. There have been recent demands for understanding the mechanisms of turbulent flames. A promising approach to the analysis of turbulent flames is to introduce conserved scalars (Linan and Williams, 1993) so that data on laminar flames can be used. Correlations of laminar flame structures on the basis of mixture fractions allow turbulent flame properties of interest to be calculated with relative simplicity. The mixture fraction, Z , for the two-feed system (oxidizer and fuel) can be defined as

$$Z = (Y_i - Y_{i2}) / (Y_{i1} - Y_{i2}) \quad (15)$$

Here Y_i is the mass fraction of the i -chemical element; the subscripts 1 and 2, respectively, refer to the composition in the fuel and the oxidizer flows. There are indications that the correlations can be approximately applied even for soot

and chemical species that are known to be out of the chemical equilibrium region (Koylu and Faeth, 1991). If the binary diffusion coefficients of all pairs of species are approximately equal, then the concentrations of all species can be uniquely related to Z through algebraic equations. If this condition is not satisfied, then different diffusion rates can cause Z for different elements (N, O, C, H) to take different values (Linan and Williams, 1993).

Here, structure of a laminar coflow methane-air diffusion flame will be introduced because methane is the simplest saturated hydrocarbon, yet it can represent the general nature of hydrocarbon-air combustion. A 20-mm-high methane-air diffusion flame, established on a 16-mm-diameter Pyrex burner, was probed by a microsampling probe, and 15 different steady chemical species were separated; concentration of each of these 15 species was measured with a gas chromatograph. Two-dimensional profiles of steady flame temperature were measured by traversing a fine thermocouple. Figure 5 shows a schematic of the laminar methane-air diffusion flame that was probed using the experimental apparatus shown in Figure 6 (Saito *et al.*, 1986). The main elements of the apparatus include a quartz coflow burner with Pyrex chimney that can produce a stable and steady laminar diffusion flame, a quartz microsampling probe that can probe chemical species from the flame, fuel and air supply and control sys-

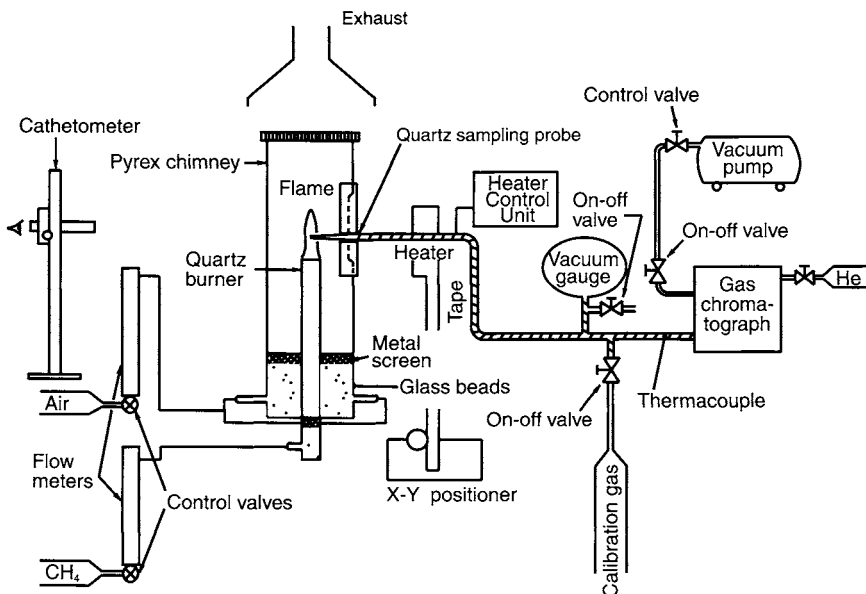


FIGURE 6 A schematic of methane-air diffusion flame experimental apparatus (Saito *et al.*, 1986).

tem, a gas chromatograph, and a cathetometer for flame height measurement. The sampling line that connects the quartz probe and gas chromatograph is wrapped with a heating tape to prevent condensation of water and heavy molecular species.

The distinctive color differences shown in the Figure 5 flame can be explained as follows. A thick blue near the burner port is associated with chemiluminescence from exited CH and CO molecules. Above that thick blue, there is a thin blue (chemiluminescence from CO) covering the entire flame. Inside the thin blue, there is yellow-soot region and on the top of that yellow-soot region, a narrow orange-soot region is formed. The yellow- and orange-soot regions are clearly separated. The two soot-color zones were found by Saito *et al.* (1987). At the yellow region, young soot particles are formed, and the soot particle temperature is higher than the gas temperature because the young soot particles can actively react with the gas molecules, causing a strong exothermic reaction on the soot particle surface. However, at the orange-soot region, young soot becomes mature and has lost its surface reactivity, bringing the soot particle and gas temperatures into equilibrium.

The centerline profiles of chemical species of the flame is shown in Figure 7. The structure of the methane-air diffusion flame, based on results from careful measurements such as Figure 7, is illustrated in Figure 8 (Linan and Williams, 1993). In Figure 8, Z_c is the stoichiometric mixture fraction, and the one-step rate function, Eq. (6), is used. At the point, $Z = Z_c$, the fuel and oxidizer are consumed at an infinite rate, releasing the maximum heat (and achieving the maximum temperature) due to the complete combustion on the stoichiometric fuel-oxidizer mixture. The mixture is fuel-lean for $Z < Z_c$ and fuel-rich for $Z > Z_c$; for both cases, temperature drops from the maximum. At or around $Z = Z_c$, an active chemical reaction is taking place by balancing with diffusion of chemical species. This region is called the reactive-diffusive zone. There are two separate zones in each side of the reactive-diffusive zone. One is the $Z < Z_c$ side where oxygen diffuses into the flame and the other is the $Z > Z_c$ side where fuel diffuses into the flame. In these (convective-diffusive) zones, no chemical reaction takes place and convection and diffusion terms control the structure.

Kinetic models have been proposed to calculate concentrations of species for methane-air flames. These models often consist of more than 200 chemical reaction steps, but simplifications are needed to understand the structure. A reduced kinetic mechanism has been proposed by carefully selecting only essential reactions. Williams proposed to use the minimum sets that can describe the main feature of the flame and apply steady state approximations in this set to obtain a reduced mechanism. Table 1 shows the proposed four-step mechanism (Linan and Williams, 1993) consisting of fuel consumption, water-gas shift, recombination, and oxygen consumption and radical production. The Table 1 results were obtained from guesswork on 14 fundamental reaction steps offered

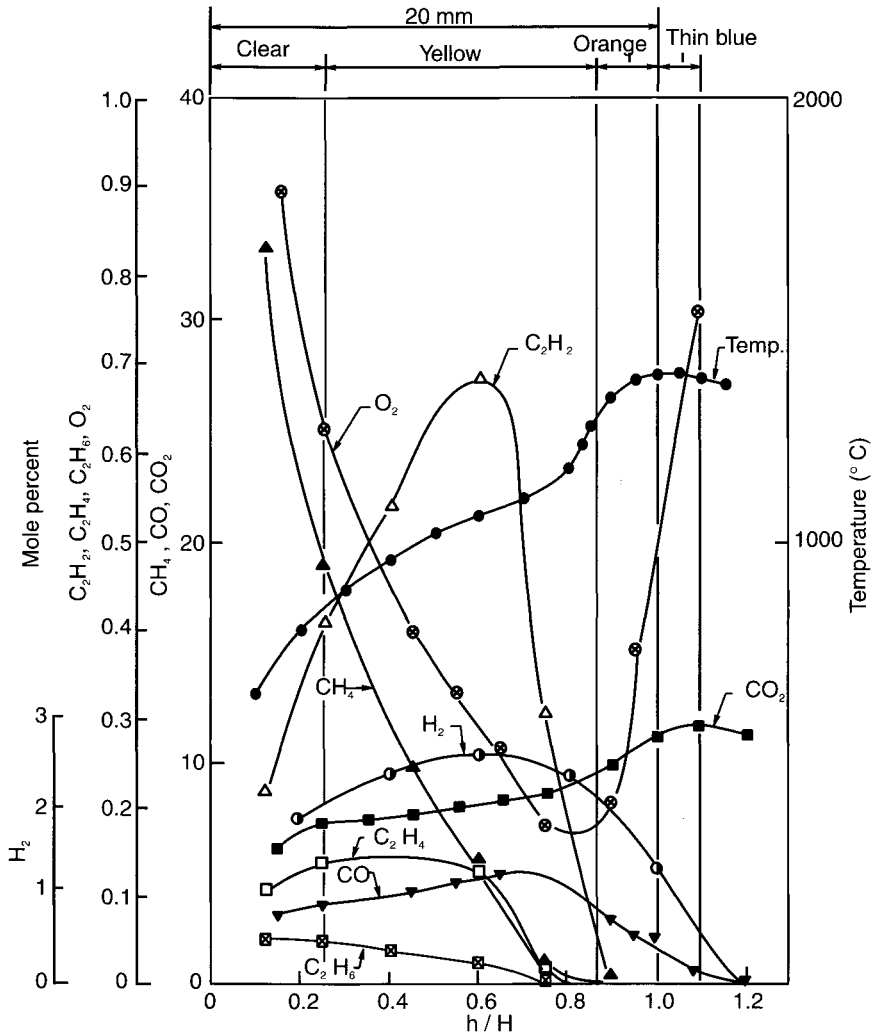


FIGURE 7 The centerline profiles of temperature and chemical species for a laminar methane-air diffusion flame established over an overventilated 1.6-cm-diameter coflow burner (Saito *et al.*, 1986).

by Linan and Williams (1993) and applying steady state approximation for the intermediaries, O, OH, HO_2 , CH_3 , CH_2O , and CHO. The usefulness of this four-step mechanism has been demonstrated. Even simpler three- or two-step mechanisms were also proven to be sufficient to explain many aspects of flame structure.

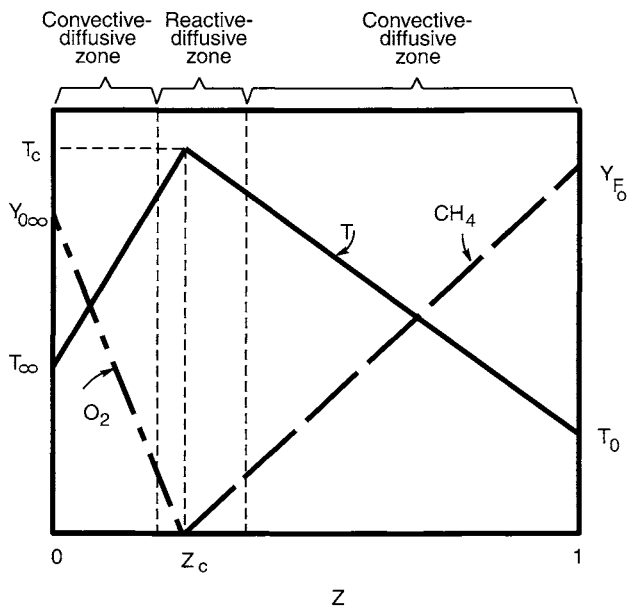


FIGURE 8 Thermal and chemical structures of the methane-air diffusion flame plotted against mixture fraction Z .

TABLE 1 Four-Step Mechanism for the Methane-Air Flame

Fuel consumption	$\begin{aligned} \text{CH}_4 + \text{H} &\rightarrow \text{CH}_3 + \text{H}_2 \\ \text{CH}_3 + \text{O} &\rightarrow \text{CH}_2\text{O} + \text{H} \\ \text{CH}_2\text{O} + \text{H} &\rightarrow \text{CHO} + \text{H}_2 \\ \text{CHO} + \text{M} &\rightarrow \text{CO} + \text{H} + \text{M} \\ \text{H} + \text{OH} &\rightarrow \text{O} + \text{H}_2 \\ \text{H} + \text{H}_2\text{O} &\rightarrow \text{OH} + \text{H}_2 \end{aligned}$
Water-gas shift	$\begin{aligned} \text{CH}_4 + 2\text{H} + \text{H}_2\text{O} &\rightarrow \text{CO} + 4\text{H}_2 \\ \text{CO} + \text{OH} &\rightleftharpoons \text{CO}_2 + \text{H} \\ \text{H} + \text{H}_2\text{O} &\rightleftharpoons \text{OH} + \text{H}_2 \\ \text{CO} + \text{H}_2\text{O} &\rightleftharpoons \text{CO}_2 + \text{H}_2 \end{aligned}$
Recombination	$\begin{aligned} \text{O}_2 + \text{H} + \text{M} &\rightarrow \text{HO}_2 + \text{M} \\ \text{OH} + \text{HO}_2 &\rightarrow \text{H}_2\text{O} + \text{O}_2 \\ \text{H} + \text{H}_2\text{O} &\rightarrow \text{OH} + \text{H}_2 \\ 2\text{H} + \text{M} &\rightarrow \text{H}_2 + \text{M} \end{aligned}$
Oxygen consumption and radical production	$\begin{aligned} \text{O}_2 + \text{H} &\rightleftharpoons \text{OH} + \text{O} \\ \text{O} + \text{H}_2 &\rightleftharpoons \text{OH} + \text{H} \\ \text{OH} + \text{H}_2 &\rightleftharpoons \text{H}_2\text{O} + \text{H} \\ \text{OH} + \text{H}_2 &\rightleftharpoons \text{H}_2\text{O} + \text{H} \\ \text{O}_2 + 3\text{H}_2 &\rightleftharpoons 2\text{H}_2\text{O} + 2\text{H} \end{aligned}$

From Linan and Williams, 1993.

D. Fr NUMBER-CONTROLLED TURBULENT DIFFUSION FLAMES WITH HIGH Pe NUMBER

When the velocity of incoming fuel jet is relatively low compared to the velocity of hot gas accelerated in the turbulent flame zone by buoyancy, a buoyancy-controlled turbulent flame will be obtained. Good examples of this type of flame are turbulent liquid pool fires, which can be created by igniting a liquid fuel placed in a relatively large diameter open top pan (say larger than 1 m for most hydrocarbon fuels and a lesser diameter for alcohol fuels). When the diameter of the pan is less than a few centimeters, the flame shape will be laminar. When the diameter is approximately between a few centimeters and 1 m, the flame will be in a transient regime between laminar and turbulent. When the diameter is larger than 1 m, the flame exhibits fully developed turbulence and often emits black smoke; sometimes the entire flame will be covered by a thick dense smoke.

Figure 9a (see color insert) shows a diesel oil fire of a 15-m² open-top container, conducted in an open field with a wind of approximately 9–12 m/s; a thick dense smoke covers almost the entire flame making the flame height measurement difficult. An infrared thermograph technique, described in the temperature measurement section, was applied to obtain a two-dimensional temporal map of flame temperatures from a remote location (Figure 9b; see color insert). Interestingly, the infrared image in Figure 9b shows the highest temperature zone for such a large-scale pool fire to be near the flame base. A similar result was found in a recent large-scale crude oil fire where an infrared (IR) thermograph was used to measure temperature distributions of a smoke-covered flame (Koseki *et al.*, 1999). It is not clear whether the result is false due to the change of emissivity of the flame or real. If it is real, it may be attributed to the enhanced cooling effect by buoyancy-induced convection of outside air in the upper portion of the flame where a large-scale puffing motion takes place.

E. SCALING LAWS

Forest fires spread nonuniformly and nonsteadily over nonhomogeneous materials. To understand complicated mechanisms of forest fires, it may be necessary to design a laboratory-scale test without changing the essential chemistry and physics governing the forest fires and measure specific aspects of forest fire behavior under well-controlled laboratory conditions. Prediction models then can be developed against these experimental data. Scale modeling is an experimental technique to realize these needs. The purpose of scale modeling is well described by Johnstone and Thring (1957): “commit your blunders on a small scale and make your profits on a large scale.” The role of scale modeling in the

study of forest fires is certainly important because many forest fire phenomena are so large that full-scale experiments are difficult to conduct due to safety conditions, economical and time constraints, as well as technical difficulty in controlling the parameters. In scaling combustion and fire phenomena, the same temperature for both the model and the full-scale may be required to make the same chemical reactions for both.

The rules that researchers must follow in setting up and interpreting the results of scale model experiments are called scaling laws or model rules (Emori and Schuring, 1977). To give a reliable forecast of full-scale phenomena, the development of scaling laws is very important, and indeed the use of scale models can be justified only if they are able to provide information relevant to the full-scale phenomena.

Governing equations can be applied to obtain strict scaling laws shown below.

$$\pi_i = \pi'_i \quad (16)$$

where π_i (pi-numbers) represent dimensionless numbers involved in the full-scale (or prototype) phenomena ($i = 1, 2, 3, \dots$), and the prime represents the scale model. Williams (1969) showed us that the strict governing equations in combustion systems yield 29 pi-numbers. Thus, it is difficult to satisfy the Eq. (16) requirement. For example, take π_1 as Reynolds number and π_2 as Froude number. Then π_1 requires the characteristic velocity to be proportional to (Length scale)⁻¹, whereas π_2 requires the characteristic velocity to be proportional to (Length scale)^{1/2}, resulting in a scaling conflict. However, if we can find reasons to neglect one of them, then the scaling problem can be resolved. Thus, the essential problem of scale modeling is to select only a few groups of pi-numbers and discard others to realize the scaling laws.

Scaling laws were derived for the last type of flames, referred to as pool fires, by employing the following assumptions (Emori and Saito, 1983): (1) the pressure is atmospheric for both model and the full-scale fire, (2) the dominant heat input to the fuel surface is given by radiation from the optically thick flame, (3) conducted heat through the rim of the pan is negligibly small, (4) inertia and buoyancy terms in the motion of gas and air are dominant compared with viscous term, and (5) the flame pulsation phenomenon is governed by the inertial and buoyant effect of combustion gas and air.

With the same ambient conditions for both the scale model and the full-scale model and with the use of the same fuel under the same ambient conditions, scaling laws were reduced to a functional relationship of the form

$$\Phi\{u_1/u_2, h/d, df/u_1, dg/u_2^2, E_r/(\rho_f q_f V_f)\} = 0 \quad (17)$$

where u_1 is the lateral wind velocity, u_2 is the buoyancy-induced velocity, h is the visible flame height, d is the diameter of the liquid pool, f is the frequency

of the flame pulsation, g is acceleration due to gravity, E_r is the radiant heat flux received by a radiometer at geometrically similar points, scaled according to the size of the fuel bed, V_f is the rate of decrease of height of fuel surface by combustion, Φ is an arbitrary function, ρ_f is the density of the fuel, and q_f is the heat value per unit mass of liquid fuel.

It was found experimentally that the regression rate V_f does not depend on the diameter of the fuel container. The burning time $t_b = h_f/V_f$, where h_f is the depth of liquid fuel in the container, does not depend on the size of container if the initial fuel thickness is the same. As a result, the condensed phase is controlled by $E_r/(\rho_f q_f V_f)$ in Eq. (17), whereas the flame behavior is governed by four other pi-numbers, u_1/u_2 , h/d , dg/u_1 , dg/u_2^2 . This is the major difference between pool fires and crib fires (to be explained in the following section), where the common group of pi-numbers governs both condensed and gas phases.

Equation (17) can be used to design scale models and determine specific experimental conditions for scale model experiments. Using h/d and dg/u_2^2 , for example, the model experiments are to be performed with wind velocities proportional to the square root of the fuel bed diameter. The scaling then predicts variations of flame height and vertical velocity in the flame. Wind tunnel fire experiments can be designed to verify these predictions (Emori and Saito, 1983).

F. WOOD CRIB FIRES

In contrast to the pool fires where the regression rate of the fuel is the same in winds of different velocities, the burning rate of wood crib fires can easily be increased by flowing air on it. Thus, scaling laws on crib fires employ the same assumptions—(1), (3), (4), and (5)—as employed for the pool fires. Assumption (2), however, is modified to account for energy transfer by buoyancy. Thus, assumption (2) for crib fires includes both radiation and convection as the dominant heat input. Figure 10 shows the configuration of a crib fire bed and a Japanese cedar crib fire. The configuration of the crib promotes three-dimensional turbulence so that the flow remains turbulent in cribs at smaller diameters than in pool fires, suggesting that the geometrical configurations play an important role in combustion.

With the use of the same crib materials and under the same ambient conditions, the pi-numbers obey a functional relationship of the form

$$\Psi\{u_1/u_2, h/l_c, l_c/u^2t, l_c g/u_2^2, E_r t/(\rho_c l_c q_c)\} = 0 \quad (18)$$

In addition to the symbols defined for pool fires, here l_c is the length of the crib stick, t is the characteristic time, Ψ is an arbitrary function, ρ_c is the density of the crib stick, and q_c is the heat value per unit mass of the crib material.

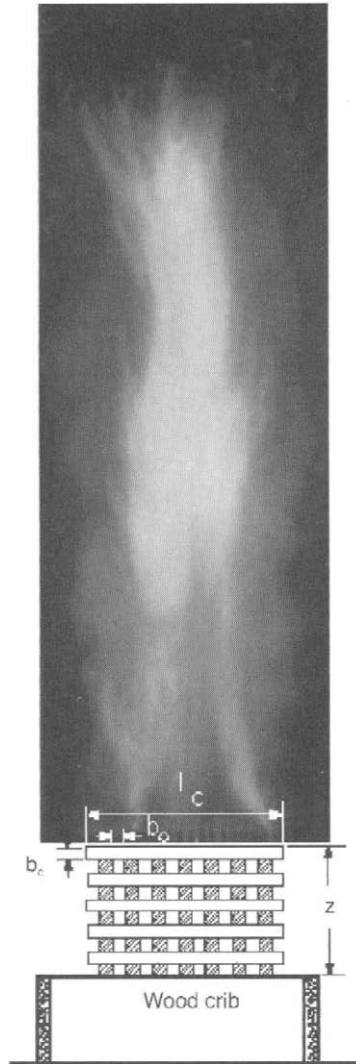


FIGURE 10 A Japanese cedar wood crib fire and crib bed configuration.

Experimental data are available to support the proposed scaling laws (Emori and Saito, 1983). Figure 11 shows that the temporal changes of irradiance from pool fires of 10 m (prototype) and 1.2 m (the scale model) in diameter become the same at corresponding times after the burning. This is consistent with the scaling law prediction, $E_r/(\rho_f q_f V_f)$, which yields $E_r/V_f = E'_r/V'_f$ and $V_f = V'_f$ for

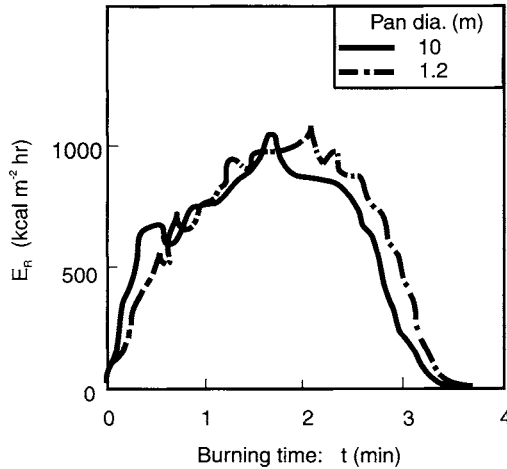


FIGURE 11 Irradiance measured at geometrically similar points as a function of time after ignition for hexane pool fires (Emori and Saito, 1983).

pool fires using the same fuel. For crib fires, the temporal change of total irradiance, both irradiance and time, are scaled to the size of the crib with $l_c = 90 \text{ cm}$ ($= l_3$) according to the scaling laws l_c/u^2t , $l_c g/u_2^2$, and $E_r t/(\rho_c l_c q_c)$. Figure 12, temporal change of total irradiance from crib fires of three different sizes, proves the scaling law predictions [Eq. (18)].

Byram and Nelson (1970) and Porscht (1975) confirmed the prediction from df/u_1 and dg/u_2^2 that the pulsating frequency becomes inversely proportional to the square root of characteristic length (e.g., diameter) of the fuel bed. Blinov and Khudyakov (1957) and Emori and Saito (1983) showed that irradiance E_r and burning time t are independent of pool diameter. Emori and Saito verified that the burning rate of a 1.2-m-diameter hexane pool fire is little influenced by lateral wind of up to 10 m/s and that the flame inclination is the same if dg/u_2^2 is kept constant.

The concept of pool and crib fires can be used to categorize the currently existing various types of fires. In forest and urban fires (Emori and Saito, 1982; Soma and Saito, 1991), for example, the heat release rate and the velocity of air is known to be respectively scaled by (Characteristic length) $^{5/2}$ and (Characteristic length) $^{1/2}$. In enclosure fires (Quintiere, 1988), such as a fire in the room of a house, the burning rate is known to depend on ventilation from openings, and the Fr number can scale the velocity of air. These fires, therefore, can be categorized as crib fires. On the other hand, a fire on a railroad passenger car was best characterized as a combination of pool and wood crib fires (Emori and Saito, 1983).

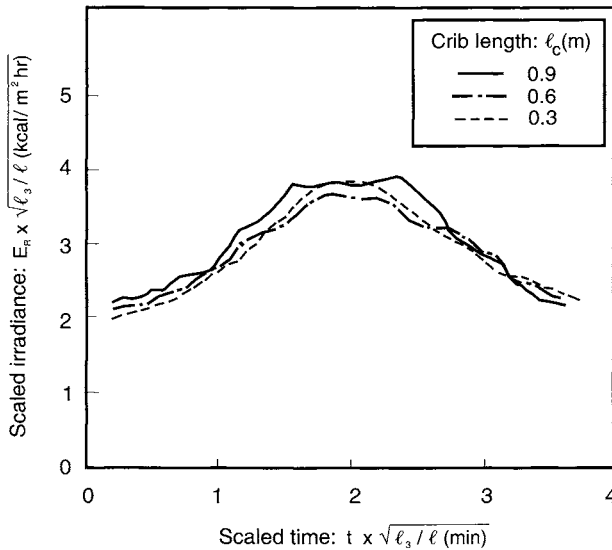


FIGURE 12 Scaled irradiance measured at a geometrically similar location as a function of scaled time for crib fires (Emori and Saito, 1983). The l is characteristic length of crib bed, and l_3 is the crib length of 90 cm. The square root relationships are based on Fr number scaling described in Eq. (18).

VII. SPREADING FLAMES

In forest and urban fires, both laminar and turbulent flame could spread either in one-dimensional, two-dimensional, or three-dimensional fuel configurations with steady or unsteady modes of spread. However, most of the fire spread modes will be turbulent with strong or minor interactions with wind. Flame spread direction can be either concurrent or opposed to the wind direction. Because of the difficulty associated with the unsteady nature of turbulence, most of the detailed measurements on spreading fires are done for a two-dimensional laminar flame with a steady state spreading rate over a one-dimensional or two-dimensional fuel surface. Theoretical models developed range from simple one-dimensional laminar steady state models to complex three-dimensional turbulent spread models (Williams, 1976; Wichman, 1992). These models, derived for and tested in well-controlled laboratory conditions, address the fundamental nature of flame spread.

The structure of spreading flames over condensed fuels, either liquid or solid, has been studied both theoretically and experimentally. A difficulty, however, lies in the transient measurement technique, which is far more difficult than

the steady-state measurements because of the highly transient nature of flame spread behavior. It has been a challenge to obtain the two-dimensional and three-dimensional profiles of chemical species concentration, velocity, and temperature for the spreading flames. Progress has been made recently by an international collaborative effort (Ito *et al.*, 1999) to use simultaneously laser sheet particle tracking (LSPT), single-wavelength (HI), or dual-wavelength (DWHI) holographic interferometer and infrared thermograph techniques. This simultaneous measurement technique made transient two-dimensional measurements of velocity, fuel concentration, and temperature for spreading flames possible. A dual-wavelength hologram was obtained for a spreading flame over propanol that was placed in a Pyrex tray 30 cm long and 1 cm wide (Ito *et al.*, 1999). Two different lasers—argon-ion and He-Ne—were used as the light source. The dual-wavelength hologram contains two different data—temperature and fuel concentrations. For the temperature holograms, each colored line represents an isothermal contour, whereas for the concentration holograms it represents equal fuel density contours. From the second hologram, the fuel vapor concentration profiles in the upstream from the spreading flame-front was obtained.

Fire spread can occur if there is communication between the burning region and the virgin fuel. With the definitions of v = the flame spread rate, q = the net energy per unit area per second transported across the surface of fire inception, and Δh = the difference in thermal enthalpy per unit mass between the fuel at its ignition and the virgin fuel, the energy balance can be written as

$$\rho_f v \Delta h = q \quad (19)$$

Flame spread can be classified based on its spreading direction (i.e., downward, horizontal and upward). Using this classification, for example, flame spread over a 15-degree angle up-slope hill can be treated as the combination of upward and horizontal spread.

Many other parameters can influence the spread rate in forest fires. Those parameters include the type of fuel (thermally thick or thermally thin solid fuel, char-forming or non-char-forming, porous, liquid, etc.), the fuel conditions (moisture contents, temperature, and aging), the size and geometry (discrete or continuous) of the fuel bed, and the ambient (wind, temperature, and humidity) conditions. Rothermel (1972) extended the flame spread equation (19) to forest fires by adding two important components, wind and fuel bed slope effects:

$$v = q/\rho_f \Delta h = I_R \xi (1 + \Phi_w + \Phi_s) / \rho_f \omega Q_{ig} \quad (20)$$

where I_R = reaction intensity, ξ = propagating flux ratio (the proportion of the reaction intensity that heats adjacent fuel particles to ignition), Φ_w = a dimensionless multiplier that accounts for the effect of wind in increasing the propa-

gating flux ratio, Φ_s = a dimensionless multiplier that accounts for the effect of slope in increasing the propagating flux ratio, ω = the effective heating number (the proportion of a fuel particle that is heated to ignition temperature at the time flaming combustion starts), and Q_{ig} = ignition energy. Here $\Delta h = \omega Q_{ig}$. Further explanation of Eq. (20) is not offered here because it is available in Rothermel (1972) and Pyne *et al.* (1996).

Williams (1982) stresses that developing a general formula to predict the spread rate including all the preceding parameters is not practical nor the best avenue. He rather suggests developing the spread rate formula for special cases and studying each case thoroughly. Taking his advice as a guide, four types of fire spread that have application to forest fires are summarized here (Williams, 1976, 1982). Note that for downward and horizontal spread, radiation is believed to become important, whereas for upward spread both radiation and convection become important.

A. DOWNWARD AND HORIZONTAL FLAME SPREAD

Types of forest fuel may be categorized as thermally thin or thermally thick. For thermally thin fuels, temperature rises across the entire cross section of the virgin fuel prior to arrival of the flame. For thermally thick fuels, the fuel interior may not be heated appreciably prior to arrival of the flame, and the temperature won't rise throughout the entire cross section of the virgin fuel prior to arrival of the flame. For downward and horizontal spread, the spread direction is opposed to the fire-induced flow direction, resulting in a slow and steady spread rate (≈ 1 cm/s or less).

Downward and horizontal spread may be associated with an early stage of flame spread in forest fires. A small circulation that was found in the gas phase just ahead of the spreading flame's leading edge may play an important role in providing heat from the flame to a virgin fuel surface (Ito *et al.*, 1999). Gas-phase heat conduction and radiation may also be important.

For forest fires, radiation from the flame may be a dominant heat transfer mode of flame spread (Albini, 1986). Applying $q = (\epsilon\sigma T^4 h) \sin \theta / \ell$ to Eq. (19), Eq. (21) will be obtained for thermally thin fuels:

$$v = (\epsilon\sigma T^4 h) \sin \theta / (\ell \rho_f \Delta h) \quad (21)$$

where h is the visible flame height, θ is the angle between the flame (usually the vertical dimension) and the exposed virgin fuel surface ($\theta > \pi/2$), and ℓ is fuel bed thickness. When the fuel is thermally thick, it won't be heated throughout its depth prior to ignition. Then, using thermal diffusivity $\alpha (= \lambda/c_p \rho_f)$, the fuel

thickness that is heated by the flame, $(\alpha h/v)^{1/2}$, can be used instead of the fuel thickness ℓ in Eq. (21). Thus, for thermally thick fuels,

$$v = (\varepsilon\sigma T^4)^2 h \sin^2 \theta / [\alpha \rho_f^2 (\Delta h)]^2 \quad (22)$$

B. TURBULENT UPWARD FLAME SPREAD

Upward flame spread occurs with a large heat release rate created by rapid (≈ 1 m/s or more) and acceleratory spread modes because the flame comes in contact with the fuel in the downstream direction effectively preheating the fuel surface by convection and radiation. Upward spread rate is much faster than downward and horizontal spread rates where buoyancy-induced flow has either negative or no effect. Saito *et al.* (1985) conducted a study of upward flame spread over vertically suspended (PMMA, wood and particle board) wall samples (0.3 m wide \times 1.2 m high \times 0.015 m thick) and formulated the spread rate. In the forest, upward flame spread will occur when a tree trunk ignites near the root and flame spreads along the trunk. Figure 13 shows a schematic of upward flame spread over a vertical wall. The spread rate is given by

$$v = 4q^2(x_f - x_p) / [\pi \lambda \rho_f c_p (T_p - T_0)^2] \quad (23)$$

where x_f is the visible flame tip height, x_p is the pyrolysis flame tip height, T_p is the ignition temperature, and T_0 is the initial fuel temperature. For a wall burning in building fires, a typical value of $q = 2$ – 2.5 W/cm². The value q may be considerably larger for forest fires where intense radiant heat is generated from the surrounding burning trees.

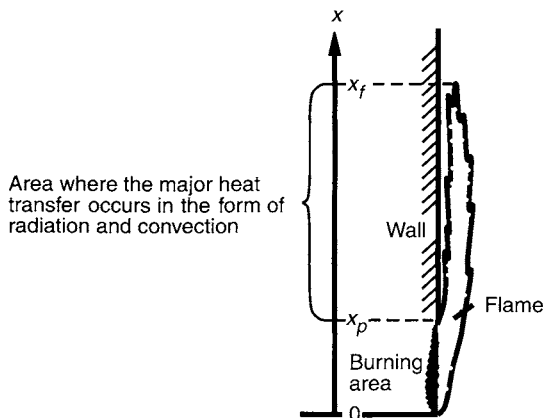


FIGURE 13 A schematic of upward flame spread over a vertical wall (Saito *et al.*, 1985).

C. FLAME SPREAD THROUGH POROUS FUEL BEDS

Forests can be treated as porous fuel beds consisting of layers of dead leaves and pine needles and thickets of trees. When these fuels are burned, flame spread occurs through the porous media fuel beds. When radiation from the burning fuel element dominates the heat transfer, Eq. (19) becomes

$$v = \varepsilon\sigma(T_f^4 - T_0^4)/f_p\rho_f(\Delta h) \quad (24)$$

where T_f is the burning fuel surface temperature, T_0 is the initial fuel temperature, and f_p is the porosity of the fuel beds. Progress has been made recently using a two-dimensional numerical calculation model to predict the maximum spotting distance in fires over porous media (McDonough *et al.*, 1998). This numerical model can accommodate variable geometrical shape of terrain and wind speed. The model prediction was roughly verified against qualitative observations made during forest fires.

Wind-aided flame spread is important in forest fires because of the enhancing effect of winds on spread rate in running crown fires (Pyne *et al.*, 1996), firebrands and spotting fires (Albini, 1979), and fire whirls and fire storms (Emori and Saito, 1982; Soma and Saito, 1991). Detailed explanations and discussions appear in Chapters 5 and 6 in this book and are also available from Albini (1981), Carrier *et al.* (1991), Wolff *et al.* (1991), and Pyne *et al.* (1996), so no further discussion is provided here.

VIII. STRUCTURE OF FLAME BASE

One of the important aspects of diffusion flames is the mechanism of flame anchoring. A commonly raised question is why and how diffusion flames are anchored. Study of the anchoring mechanism of diffusion flames is important because of its connection to fire extinguishment, control of fire spread, and flame instability. Here, two different mechanisms of flame anchoring will be explained: one sustains Fr number controlled pool fires and the other sustains Re number-controlled turbulent jet diffusion flames. Figure 14 shows an LSPT experimental apparatus applied to a small-scale pool fire. Flame-induced flow near and around the flame leading edge where the pool fire is anchored was visualized by the LSPT technique. Figure 15 shows a two-dimensional flow structure visualized by the LSPT technique for a 45-mm-diameter propanol pool fire (Venkatesh *et al.*, 1996).

For the Re number-controlled turbulent jet diffusion flames, the mechanism of anchoring depends on the formation of shear-stress-related circulation zones. Because of the shearing between the fuel jet, whose flow speed may be much higher than the flame propagation speed, and the oxidizer, a stagnant circulation

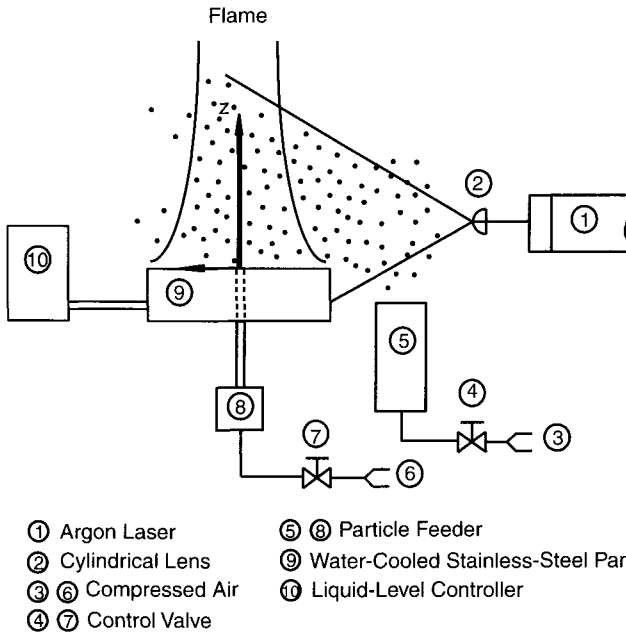


FIGURE 14 Schematic of a laser sheet particle tracking system applied to a small-scale propane pool fire.

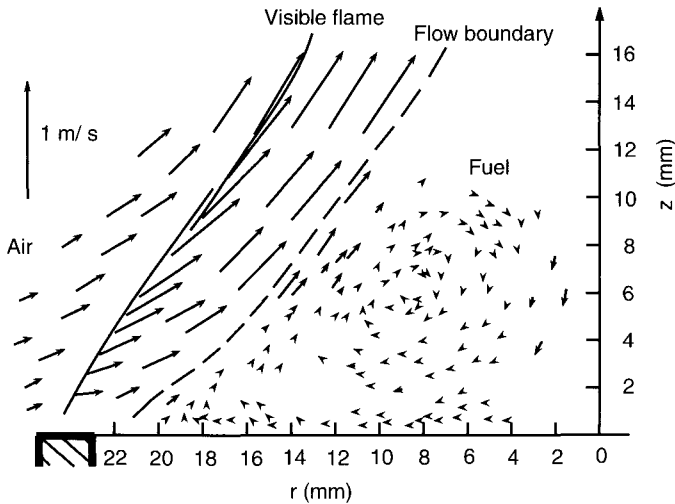


FIGURE 15 A two-dimensional flow structure of the flame base obtained by the LSPT technique shown in Figure 14. Center of the flame base is at $r = 0$.

zone is developed where mixing occurs and the flame is allowed to anchor. For pool fires, the shear stresses at the rim are lower by two orders of magnitude compared to the jet diffusion flame, demonstrating the insignificance of shear-stress-induced mixing and suggesting the presence of a molecular-diffusion-mixing zone due to finite-rate chemistry. Nevertheless, both anchoring mechanisms require the generation and sustained presence of a mixing zone, where fuel and oxidizer can intermix. The mechanisms by which these two flames produce these zones are quite distinct.

The structure of the flame leading edge where the pool fire is anchored is similar to that of a spreading flame. Because of finite-rate chemistry influences, the flame sheet has a finite thickness. Because the diffusion flame is bounded on either side by two premixed flames (Figure 8), the concept of the premixed flame propagation speed (described earlier) can be applied. The direction of the flame propagation is opposite to the tangential component of the air entrainment vector, V_t . If V_t is greater than the flame propagation speed near the base, the flame will not be able to anchor or stabilize. The LSPT measurements, shown in Figure 15, confirmed that V_t in the convective-air entrainment zone was lower than the stoichiometric flame speeds for the anchored pool fire. For the flame with V_t higher than the stoichiometric flame speed, however, the flame was no longer able to anchor the burner port resulting in lift-off or blow-off, which led to extinction. A schematic of structure of diffusion flames shown in Figure 8 also provides additional explanation. The flame is able to spread when the oxidizer and fuel mixture is in the reactive-diffusive zone; the spread rate is maximum at $Z = Z_c$ and becomes slower both at $Z < Z_c$ and at $Z > Z_c$.

IX. CONCLUSIONS

Topics introduced in this chapter cover a small portion of flame studies that have been accomplished in the past. Some interpretations given here are the author's view and subject to further discussion. The intention of the author is to discuss fundamentals of combustion and to stimulate readers to think scientifically when they deal with forest fire problems. References are provided for readers who are interested in advancing their understanding in flames and combustion.

ACKNOWLEDGMENTS

Ralph Nelson read the manuscript and offered many valuable comments. This author is largely indebted to Forman Williams and Alvin Gordon who taught principles of combustion and have

been the constant source of education. This work is sponsored both by Kentucky-NASA EPSCoR program and Trinity Industrial Corporation through a general education gift.

NOTATION

ROMAN LETTERS

A	pre-exponential factor	s^{-1}
\tilde{A}	cross-sectional area of the slab	m^2
D	binary diffusion coefficient of a fuel into air	$m^2 s^{-1}$
E	activation energy	$J mol^{-2}$
E_r	radiant heat flux received by a radiometer of geometrically similar points	$W m^{-2}$
F	body force	N
H	minimum ignition energy	J
H_o	energy per unit mass added to the mixture by the combustion	$J g^{-1}$
I_R	reaction intensity	$W m^{-2}$
PCC	product of complete combustion	
PICC	product of incomplete combustion	
Q	heat of combustion	J
Q_{ig}	ignition energy	J
T	temperature	K
T_a	gas temperature surrounding the thermocouple	K
T_b	thermocouple bead temperature	K
T_o	the initial temperature	K
T_f	burning fuel surface temperature	K
T_p	ignition temperature	K
T_∞	the final temperature	K
T_S	shear stress tensor	P_a
V_f	the rate of decrease of height of fuel surface by combustion	$m s^{-1}$
V_t	the tangential component of the air entrainment vector	$m s^{-1}$
Y_F	mass fraction of fuel	

Y_i	mass fraction of the i -chemical element	
Y_{i1}	mass fraction of the i -chemical species in the fuel	
Y_{i2}	mass fraction of the i -chemical species in the oxidizer	
Y_O	mass fraction of oxidizer	
Z	mixture fraction	
Z_c	stoichiometric mixture fraction	
a	absorption coefficient of gas surrounding the thermocouple	
c_p	specific heat at constant pressure	$\text{J K}^{-1} \text{mol}^{-1}$
d	burner port diameter or diameter of liquid pool	m
f	frequency of the flame pulsation	s^{-1}
f_p	porosity of the fuel beds	
g	acceleration due to gravity	m s^{-2}
h	visible flame height	m
h_f	depth of liquid fuel	m
Δh	the difference in thermal enthalpy per unit mass between the fuel at its ignition and the virgin fuel	J g^{-1}
k	specific reaction rate constant	s^{-1}
l	characteristic length	m
ℓ	fuel bed thickness	m
l_3	90 cm	
l_c	crib stick length	m
l_T	a characteristic length related to the high temperature gradient in the gas	m
m, n	reaction order	
p	pressure over characteristic pressure	
q	the net energy per unit area per second transported across the surface of fire inception	W cm^{-2}
q_c	heat value per unit mass of the crib material	J g^{-1}
q_{cod}	conduction heat loss	W m^{-2}
q_{cov}	convection heat loss	W m^{-2}
q_f	heat value per unit mass of liquid fuel	J g^{-1}
q_{rad}	radiation heat loss	W m^{-2}
t	characteristic time	s

t_b	h_f/V_f	s
t_c	chemical time	s
t_r	residence time	s
u_0	fuel exit velocity	m s^{-1}
v	flame spread rate	m s^{-1}
v_0	laminar burning velocity	m s^{-1}
u_1	lateral wind velocity	m s^{-1}
u_2	buoyancy-induced velocity	m s^{-1}
\hat{u}	velocity vector over characteristic velocity	
w	production rate (mass per unit volume per unit time) of chemical species by chemical reaction	$\text{g m}^{-3}\text{s}^{-1}$
x_f	the visible flame tip height	m
x_p	the pyrolysis height	m

GREEK LETTERS

Φ	an arbitrary function	
Φ_w	a dimensionless multiplier that accounts for the effect of wind in increasing the propagating flux ratio	
Φ_s	a dimensionless multiplier that accounts for the effect of slope in increasing the propagating flux ratio	
Ψ	an arbitrary function	
α	thermal diffusivity	$\text{m}^2 \text{s}^{-1}$
δ	adiabatic laminar flame thickness	m
ϵ_b	emissivity of the thermocouple bead	
λ	thermal conductivity of gas	$\text{W m}^{-1} \text{K}^{-1}$
ν	kinematic viscosity	$\text{m}^2 \text{s}^{-1}$
π	pi-number	
ρ_c	density of the crib stick	g m^{-3}
ρ_f	density of fuel	g m^{-3}
ρ_0	the initial density of the mixture	g m^{-3}
Q	density over characteristic density	
ϖ	ratio of low time to evolution time	
ω	the effect of heating number	

ξ	propagating flux ratio, the portion of the reaction intensity that heats adjacent fuel particles to ignition	
$\dot{\eta}$	heat transfer coefficient	$\text{W m}^{-2} \text{K}^{-1}$

DIMENSIONLESS GROUPS

D_{IG}	critical Da number for ignition
D_{EX}	critical Da number for extinction
Fr	Froude number
M	Mach number
Pe	Peclet number
Re	Reynolds number

CONSTANTS

σ	Stefan–Boltzmann constant
R_o	universal gas constant

REFERENCES

- Albini, F. A. (1979). "Spot Fire Distance from Burning Trees—A Predictive Model." General Technical Report INT 56, Intermountain Forest and Range Experiment Station, Forest Service, USDA, Ogden.
- Albini, F. A. (1981). A model for the wind-blown flame from a line fire. *Combustion and Flame* **43**, 155–174.
- Albini, F. A. (1986). Wildland fire spread by radiation—A model including fuel cooling by natural convection. *Combustion Science and Technology* **45**, 101–113.
- Arakawa, A., Saito, K., and Gruver, W. A. (1993). Automated infrared imaging temperature measurement: With application to upward flame spread studies. *Combustion and Flame* **92**, 222–230.
- Babrauskas, V. (1988). "Handbook of Fire Protection Engineers." SFPE, Boston.
- Ban, H., Venkatesh, S., and Saito, K. (1994). Convection-diffusion controlled micro-diffusion flames. *J. Heat Transfer* **116**, 954–959.
- Benson, S. W. (1960). "The Foundations of Chemical Kinetics." McGraw-Hill, New York.
- Blinov, V. I., and Khudyakov, G. N. (1957). Certain laws governing diffusion flames in liquids. *Academiia, Nauk, USSR, Doklady* **113**, 1094–1098.
- Byram, G. M., and Nelson, R. M., Jr. (1970). The modeling of pulsating fires. *Fire Tech.* **6**, 102–110.
- Carrier, G. F., Fendell, F. E., and Wolff, M. F. (1991). Wind-aided fire spread across arrays of discrete fuel elements. I. Theory. *Combust. Sci. Tech.* **75**, 31–51.
- Clark, T. L., Coen, J. L., Radke, C. L., Reeder, M., and Packham, D. (1998). Coupled atmosphere-fire dynamics. In "Third International Conference of Forest Fire Research," pp. 67–82. Coimbra, Portugal.

- Clark, T. L., Radke, L., Coen, J., and Middleton, D. (1999). Analysis of small-scale convective dynamics in a crown fire using infrared video camera imagery. *J. Appl. Meteorol.* **38**, 1401–1420.
- Delichatsios, M. A., and Saito, K. (1991). Upward fire spread: Key flammability properties, similarity solutions and flammability indices. In "Fire Safety Science—Proceedings of Third International Symposium" (G. Cox and B. Langford, Eds.), pp. 217–226. Elsevier Applied Science, London.
- Delichatsios, M. A., Delichatsios, M. M., Lougheed, G. D., Crampton, G. P., Qian, C., Ishida, H., and Saito, K. (1995). Effect of external radiant heat flux on upward fire spread: Measurements on plywood and numerical predictions. In "Fire Safety Science—Proceedings of the Fourth International Symposium" (T. Kashiwagi, Ed.), pp. 421–432. International Association for Fire Safety Science, Washington.
- Demtroder, W. (1982). "Laser Spectroscopy." Springer-Verlag, New York.
- Dobbins, R. A., and Megaridis, C. M. (1987). Morphology of flame-generated soot as determined by thermophoretic sampling. *Langmuir* **3**, 254–259.
- Emori, R. I., and Schuring, D. J. (1977). "Scale Models in Engineering." Pergamon Press, London.
- Emori, R. I., and Saito, K. (1982). Model experiments of hazardous forest fire whirl. *Fire Tech.* **18**, 319–327.
- Emori, R. I., and Saito, K. (1983). A study of scaling laws in pool and crib fires. *Combust. Sci. Tech.* **31**, 217–230.
- Faraday, M. (1993). "The Chemical History of a Candle." Cherokee Pub., Atlanta.
- Ferguson, E. S. (1993). "Engineering and the Mind's Eye." The MIT Press, Cambridge.
- Fernandez-Pello, A. C. (1995). The solid phase. In "Combustion Fundamentals of Fire" (G. Cox, Ed.), Chapter 2, pp. 31–100. Academic Press, San Diego.
- Fristrom, R. M., and Westenberg, A. A. (1985). "Flame Structure," 2nd ed. McGraw-Hill, New York.
- Gaydon, A. G., and Wolfhard, H. G. (1979). "Flames: Their Structure, Radiation and Temperature," 4th ed. Chapman Hall, London.
- Glassman, I. (1996). "Combustion," 3rd ed. Academic Press, San Diego.
- Hirano, T. (1986). "Combustion Physics." Kaibundo, Tokyo. (In Japanese.)
- Hirano, T., and Saito, K. (1994). Flame spread phenomena: The role of observation in experiments. *Progr. Energy Combust. Sci.* **20**, 461–485.
- Ito, A., and Kashiwagi, T. (1988). Characterization of flame spread over PMMA using holographic interferometry: Sample orientation effects. *Combustion and Flame* **71**, 189–204.
- Ito, A., Konishi, T., Narumi, A., Tashitouch, G., Saito, K., and Cremers, C. J. (1999). The measurement of transient two-dimensional profiles of velocity and fuel concentration over liquids. *J. Heat Transfer* **121**, 413–419.
- JANAF. (1985). "Thermochemical Tables," 3rd ed. (M. W. Chase, Jr., et al., Eds.). J. Physical and Chemical Reference Data.
- Johnstone, R. E., and Thring, M. W. (1957). "Pilot Plants, Models, and Scale-up Methods in Chemical Engineering." McGraw-Hill, New York.
- Kashiwagi, T. (1994). Polymer combustion and flammability—Role of condensed phase. In "Twenty-fifth International Symposium on Combustion," pp. 1423–1437. The Combustion Institute, Pittsburgh.
- Koseki, H., Iwata, Y., Natsume, Y., Takahashi, T., and Hirano, T. (1999). Tomakomai large scale crude oil fire experiments. *Fire Tech.* **36**, 24–38.
- Koylu, U. O., and Faeth, G. M. (1991). Carbon monoxide and soot emission from liquid-fueled buoyant turbulent diffusion flames. *Combust. Flame* **87**, 61–76.
- Linan, A., and Williams, F. A. (1993). "Fundamental Aspects of Combustion." Oxford University Press, New York.
- Long, R. T., Jr., Torero, J. L., Quintiere, J. G., and Fernandez-Pello, A. C. (2000). Scale and trans-

- port considerations on piloted ignition of PMMA. In "Fire Safety Science—Proceedings of Sixth International Symposium." The International Association for Fire Safety Science, Washington.
- Majidi, V., Saito, K., Gordon, A. S., and Williams, F. A. (1999). Laser-desorption time-of-flight mass-spectrometer analysis of soot from various hydrocarbon fuels. *Combust. Sci. Tech.* **145**, 37–56.
- McDonough, J. M., Garzon, V. E., and Saito, K. (1998). "A Porous Medium Model of Turbulent Wind-driven Wildland Fires." Department of Mechanical Engineering Internal Report, University of Kentucky, Lexington, KY.
- Mulholland, G., Liggett, W., and Koseki, H. (1996). The effect of pool diameter on the properties of smoke produced by crude oil fires. In "Twenty-sixth International Symposium on Combustion," pp. 1445–1452. The Combustion Institute, Pittsburgh.
- Orloff, L., de Ris, J. N., and Markstein, G. H. (1975). Upward turbulent flame spread and burning of fuel surface. In "Fifteenth International Symposium on Combustion," pp. 183–192. The Combustion Institute, Pittsburgh.
- Porscht, R. (1975). Studies on characteristic fluctuations of the flame radiation. *Combust. Sci. Tech.* **10**, 73–76.
- Pyne, S. J., Andrews, P. L., and Laven, R. D. (1996). "Introduction to Wildland Fire," 2nd ed. John Wiley & Sons, New York.
- Quintiere, J. G. (1988). "Handbook of Fire Protection Engineers." SFPE, Boston.
- Quintiere, J. G. (1998). "Principles of Fire Behavior." Delmar Pub., Albany, NY.
- Radke, L. F., Clark, T. L., Coen, J. L., Walter, C., Riggan, P. J., Brass, J., and Higgins, R. (1999). Airborne remote sensors look at wildland fires. In "Fourth International Airborne Remote Sensing Conference and Exhibition/ 21st Canadian Symposium on Remote Sensing." Ottawa.
- Rashbash, D. J. (1962). The extinction of fires by water sprays. *Fire Res. Abstr. Rev.* **4**, 28–53.
- Rothermel, R. C. (1972). "Mathematical Model for Predicting Fire Spread in Wildland Fuels." Res. Pap. INT-115, Intermountain Forest and Range Experiment Station, Forest Service, USDA, Ogden.
- Sabersky, R. H., Acosta, A. J., and Hauptman, E. G. (1989). "Fluid Flow," 3rd ed. Macmillan, New York.
- Saito, K., Quintiere, J. G., and Williams, F. A. (1985). Upward turbulent flame spread. In "Fire Safety Science—Proceedings of the First International Symposium," pp. 75–86. Hemisphere Pub., Washington.
- Saito, K., Williams, F. A., and Gordon, A. S. (1986). Structure of laminar co-flow methane-air diffusion flames. *J. Heat Transfer* **108**, 640–648.
- Saito, K., Gordon, A. S., and Williams, F. A. (1987). A study of two-color soot zone for small hydrocarbon diffusion flames. *Combust. Sci. Tech.* **51**, 291–312.
- Saito, K., Wichman, I. S., Quintiere, J. G., and Williams, F. A. (1989). Upward turbulent flame spread on wood under external radiation. *J. Heat Transfer* **111**, 438–445.
- Saito, K., Gordon, A. S., Williams, F. A., and Stickle, F. A. (1991). A study of the early history of soot formation in various hydrocarbon diffusion flames. *Combust. Sci. Tech.* **80**, 103–119.
- Soma, K., and Saito, K. (1991). Reconstruction of fire whirls using scale models. *Combust. Flame* **86**, 269–284.
- Takahashi, F., Vangsness, M. D., Durbin, M. D., and Schmoll, W. J. (1996). Structure of turbulent hydrogen jet diffusion flames with or without swirl. *J. Heat Transfer* **118**, 877–884.
- Tewarson, A., and Ogden, S. D. (1992). Fire behavior of polymethylmethacrylate. *Combustion and Flame* **89**, 237–259.
- Venkatesh, S., Ito, A., Saito, K., and Wichman, I. S. (1996). Flame-base structure of small scale pool fires. In "Twenty-Sixth International Symposium on Combustion," pp. 1437–1443. The Combustion Institute, Pittsburgh.

- Wichman, I. S. (1992). Theory of opposed-flow flame spread. *Progr. Energy Combust. Sci.* **18**, 553–593.
- Williams, F. A. (1969). Scaling mass fires. *Fire Res. Abstr. Rev.* **11**, 1–23.
- Williams, F. A. (1976). Mechanisms of flame spread. In “Sixteenth International Symposium on Combustion,” pp. 1281–1294. The Combustion Institute, Pittsburgh.
- Williams, F. A. (1982). Urban and wildland fire phenomenology. *Progr. Energy Combust. Sci.* **8**, 317–354.
- Williams, F. A. (1985). “Combustion Theory.” Benjamin/Cummings, San Francisco.
- Williams, F. A. (1992). The role of theory in combustion science. In “Twenty-Fourth International Symposium on Combustion,” pp. 1–17. The Combustion Institute, Pittsburgh.
- Williams, J. M., and Gritz, L. A. (1998). In situ sampling and transmission electron microscope analysis of soot in the flame zone of large pool fires. In “Twenty-Seventh International Symposium on Combustion,” pp. 2707–2714. The Combustion Institute, Pittsburgh.
- Wilson, E. B., Jr. (1954). “An Introduction to Scientific Research.” McGraw-Hill, New York.
- Wolff, M. F., Carrier, G. F., and Fendell, F. E. (1991). Wind-aided fire spread across arrays of discrete fuel elements. II. Experiments. *Combust. Sci. Tech.* **77**, 261–289.
- Zabetakis, M. G. (1965). “Flammability Characteristics of Combustible Gases and Vapors.” U.S. Bureau of Mines, Bulletin #627, Washington.